Multimodal sensor suite for identification of flow regimes and estimation of phase fractions and velocities – Machine learning algorithms in multiphase flow metering and control

Noorain Syed Kazmi [a,*], Ru Yan [a], Saba Mylvaganam [a], Håkon Viumdal [a]

[a] *University of South-Eastern Norway, Faculty of Technology, Natural Sciences and Maritime Sciences, Dept. EE, IT and Cybernetics, Kjølnes Ring 56, 3918 Porsgrunn, Norway*

* 238758@usn.no

Abstract

Multiphase flow metering is a challenging task because of the complexity of multiphase flow. In this paper, non-intrusive multiphase flow metering techniques, including machine learning (ML) / artificial intelligence models for the identification of flow regimes and estimation of flow parameters of a two-phase flow in a horizontal pipe are proposed that use data from Electrical Capacitance Tomography (ECT) and conventional measurements such as differential pressure in the pipe. The flow regimes are classified into five types, namely plug, slug, annular, wavy and stratified. Two-phase air/water flow experimental data from ECT are collected by running extensive experiments using the horizontal section of the multiphase flow rig at the University of South-Eastern Norway (USN). Exploratory data analysis (EDA) is performed on these data to extract features for use in classification and regression algorithms. Time series of normalized capacitance data from ECT sensors are used to classify flow regimes and identify flow parameters. ML techniques of Artificial Neural Network, Support Vector Machine (SVM), K-Nearest Neighbors (KNN) and Decision Tree (DT) are used to classify flow regimes by using features extracted from ECT data. The cross-correlation technique is used to estimate flow velocity using data from a twin-plane ECT module. ML regression techniques are used to estimate phase fractions. Fusing data from differential pressure sensors enhances the flow regime classification. An overall system performance is given with suggestions for designing dedicated control algorithms for actuators used in multiphase flow control.

1. Introduction

In fluid mechanics, multiphase flow is the flow of two or more phases of matter in a pipe. Multiphase flow is a complex phenomenon. Two-phase flow is a flow where two phases out of solid, liquid and gas phases are observed simultaneously in a pipeline. Gas/Solid is prevalent in pneumatic conveyors, dust collectors, fluidized beds, heterogeneous reactors and metallized propellant rockets. Gas/liquid flow can be seen in atomizers, scrubbers, dryers and combustors. Liquid/liquid droplet flow is observed in extraction, homogenizing and emulsifying. Liquid/solid is present in flotation and sedimentation (Soo, 1990).

The geometric distribution of constituent phases in a multiphase flow is known as flow regime or pattern (Tan and Dong, 2023). There are various types of flow regimes. Slug, plug, stratified, annular, wavy, bubble, etc., are common and well-known flow regimes observed in multiphase flow (Vohr, 1960). Flow regimes depend on the orientation of pipe and direction of flow. The density of phases, viscosity of phases and mass flow rates of phases also greatly affect the creation of flow regimes (Alssayh et al., 2013). Operating pressure, temperature, valves and bends have a direct effect on the flow regimes (Hansen et al., 2019). Classification of flow regimes in a two-phase flow pipeline is a major challenge in the field of flow analysis (Pereyra et al., 2012). Flow regimes can be classified subjectively through graphics or by employing the probability density function of pressure or void fractions signals from sensors (Almalki and Ahmed, 2020; Godfrey Nnabuife et al., 2021). Flow regimes has direct effect on the measurement of flow velocities, phase fractions and other parameters (Godfrey Nnabuife et al., 2021). Some of the flow regimes observed in horizontal gas/liquid multiphase flows are described below:

- Stratified

When gas and liquid flow rates are low, stratified flow is observed. It is applicable in horizontal flow direction. There is no mixing of the two phases and the liquid phase remains as a film at the lower portion of the pipe (Liné and Fabre, 2011).

- Wavy

At higher gas flow rates, the stratified flow converts to wavy flow in which ripples or waves are observed on the top of the liquid layer. It appears like waves in a sea. (Jayanti, 2011)

- Annular

At higher gas velocity, wavy flow converts to annular flow in which liquid flows at the periphery of the pipe while gas flows at the center of the pipe. (Zeigarnik, 2011)

- Plug / Elongated Bubble

Plug is a kind of flow pattern in which large bubbles of gas float on the top surface of the liquid phase spanning a large area in the pipe. The gas phase is dispersed in the liquid phase. (Vohr, 1960)

- Slug

Slug flow is intermittent flow in which slugs of liquid with dispersed bubbles flow along with large gas pockets. The flow is always unsteady. The bubble is in the shape of a bullet. This flow alternates between high liquid fraction and high gas fraction. (Vohr, 1960)

(Wang and Zhang, 2009) use an ECT for identifying flow regimes by applying Support Vector Machine (SVM) to classify flow regimes and Principal Component Analysis (PCA) to optimize the inputs to the SVM model. (Ameran *et al*., 2015) discuss velocity measurement of two-phase flow through ECT using cross-correlation techniques. A study of flow velocity and phase concentrations of horizontal two-phase flow is presented by (Stavland *et al.*, 2021), employing a dual-plane ECT with gamma-ray tomography to measure volumetric flow rates of the phases, achieving an accuracy of ±10%.

The results presented in this paper are developed during the master thesis's work of (Noorain Syed Kazmi, 2023).

2. System Description

A multiphase flow rig is at the University of South-Eastern Norway (USN), Campus Porsgrunn. This rig is equipped with facilities for multiphase flow studies–using water, air, and mineral oil through a horizontal pipe. The pipe can be tilted by ±10º with respect to the horizontal surface. The operational limit of mass flow rate for air is 5 kg/min, whereas for liquid is 150 kg/min. By injecting various combinations of air, water and oil mass flow rates, different flow regimes can be generated and visually inspected through the Plexiglass transparent section, as shown in Fig. 1. A simplified piping and instrumentation diagram (P&ID) of the flow rig is shown in Fig. 2. Some important parameters of the rig are given in Tab. 1.

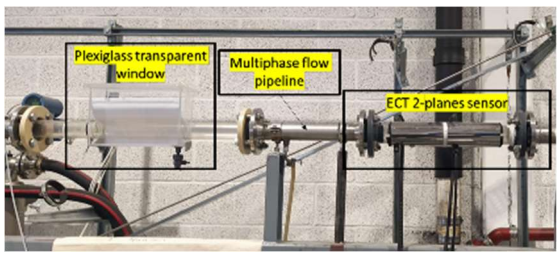

Figure 1: The rig setup (partly) at USN, Porsgrunn.

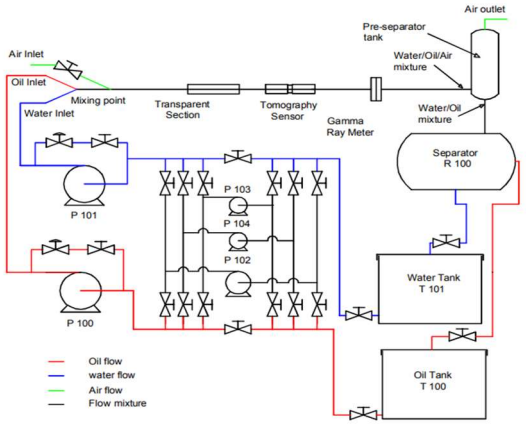

Figure 2: P&ID of the rig at USN, Porsgrunn

Table 1: Some parameters of the rig at USN, Porsgrunn

USN Flow Rig	
Inside pipe diameter	56 mm
Outside pipe diameter	60 mm
Length of pipe	15 m
Water density	996 kg/m3 at 27ºC and 1bar
Air density	1 kg/ m3
Oil density	790 kg/m3
Water viscosity	0.00102 Pa-s (20ºC)
Oil viscosity	0.00164 Pa-s (25ºC)

As depicted in Fig. 1, a TOMOFLOW TFLR5000 dual-plane ECT system from Process Tomography Limited is equipped on the rig. The ECT system can measure the flow parameters of an uneven two-phase flow when the constituents have dielectric properties (Process Tomography Limited, 2011). In this rig, air, oil and water permittivities are 1, 2.7 and 80, respectively (Dupré et al., 2017).

PDT120 and PDT121 are the differential pressure meters mounted on the rig, as shown in Fig. 3. PDT120 measures the differential pressure across a span of 10.22m in the pipe, and PDT121 captures the differential pressure across a shorter distance of 5.38m within the same pipe. In addition, the inlet air flow rate and air pressure are measured separately by a flow transmitter FT131 and a pressure transmitter PT131.

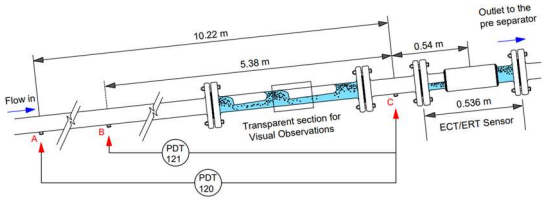

Figure 3: Measurement areas of differential pressure meters on the flow rig at USN, Porsgrunn (Dupré et al., 2017)

3. Electrical Capacitance Tomography

ECT is a non-invasive, non-radioactive flow sensing method that measures the spatial distribution of dielectric materials within a pipe using capacitance readings from peripheral electrodes (Process Tomography Limited, 2011; Saied and Meribout,

2016). The capacitances can also be converted into images for visual depiction of the flow.
Generally used in two-phase liquid/gas flow, ECT measures permittivity distribution inside a pipe at two cross-sections of a pipe that can give the velocity profile of flow while also providing volume ratio or phase fraction data. ECT is most effective when working with fluids that have low electric conductivity and variable permittivity (Process Tomography Limited, 2011). The working principle of an ECT (one plane) is shown in Fig. 4.

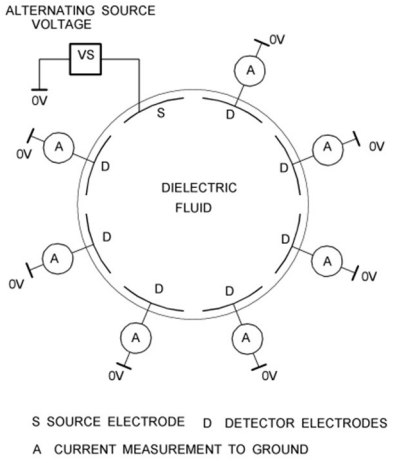

Figure 4: Principal of ECT with 8-electrodes (Process Tomography Limited, 2011)

An alternating voltage is applied between the source and the ground. The source is charged to one electrode. Currents, in direct proportion to the capacitance, are subsequently measured at all remaining electrodes. Within a single measurement frame, the currents/ capacitances between each pair of electrodes are measured. For an *N*-electrodes ECT plane, there are in total $M = N(N-1)/2$ unique capacitance values per measurement frame (Process Tomography Limited, 2011). The measured capacitances can be normalized by using Eq. 1.

$$C_n = \frac{C_m - C_L}{C_h - C_L} \qquad (1)$$

In Eq. 1, C_m is the inter-electrode raw capacitance. C_L is the capacitance when the pipe is full with lower permittivity material such as air. C_h is the capacitance when the pipe is full with higher permittivity material such as water. C_n is the normalized capacitance. C_n is dimensionless and normalized, making it suitable as input for mathematical operations and algorithms.

4. Experiments

Based on the flow conditions outlined in Fig. 5, 45 of two-phase air and water experiments are carried out on the flow rig using the ECT system. Conventional measurements such as differential pressure, temperature and mass flow rate were also recorded during each experiment.
The flow regimes indicated in Fig. 5 are validated via visual inspection throughout the experiments. Fig. 6 displays the active experimental area on the flow regime map. The lowest flow rates for air and water are 0.07 kg/min and 2 kg/min, respectively, while the highest flow rates for both mediums reach 5 kg/min and 77 kg/min. Fig. 7 illustrates the setup of the sensor array, comprising of 8 electrodes, around the pipe. Tab. 2 provides the parameters setup in the ECT system during the experiments.

Test Matrix		Water (kg/min)					
		2	3	4	75	76	77
Air (kg/min)	0.07				P	P	P
	0.09				P	P	P
	0.1	ST	ST	ST			
	0.11				P	P	P
	0.13				P	P	P
	0.15	ST	ST	ST	P	P	P
	0.3				S	S	S
	0.4				S	S	S
	0.5	ST	ST	ST	S	S	S
	1	W	W	W			
	2.5	W	W	W			
	4	A	A	A			
	5	A	A	A			
ST: Stratified; W: Wavy; A: Annular; P: Plug; S: Slug							

Figure 5: Test matrix for two-phase flow with varying velocities of water and air (in kg/min) generating different flow regimes

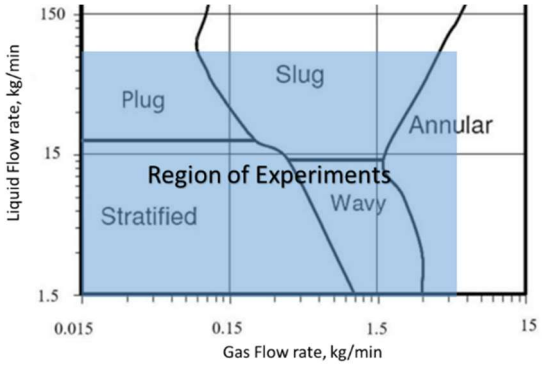

Figure 6: Active region (blue area) of experiments on a flow regime map, based on Mandani et al..

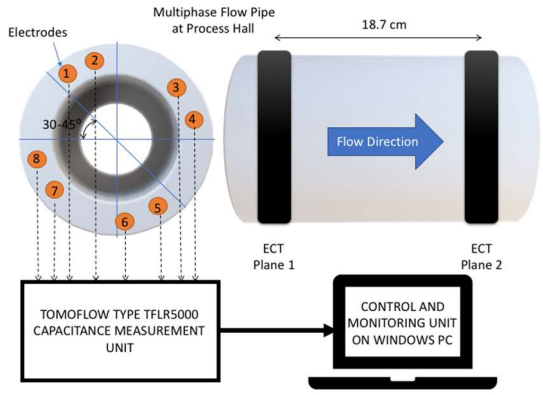

Figure 7: Setup of ECT electrodes and planes on the pipe and their connection to TOMOFLOW TFLR5000 system

Table 2: HW/SW related parameters used in the ECT module for the experiments

Parameter	Value
Frames per second per plane	100
Sampling interval per plane (ms)	10
Number of planes	2
Number of electrodes per plane	8
Number of capacitances per measured frame	28
Logging duration per experiment (s)	30

For each experiment, 3000 frames of ECT data were collected. For example, one of the experiments for Annular flow regime was conducted by simulating an Annular flow in the USN flow pipeline by using the matrix of Fig. 5. This experiment generated 3000 frames of normalized capacitances from the eight electrodes. This batch of frames was labeled as Annular to be used for supervised machine learning algorithms. Each frame consists of 28 capacitance values. For 45 experiments, a total of 135000 frames of capacitance data are collected. These capacitance data were normalized before using them in classification and regression algorithms. Each frame was flattened to 28 columns of normalized capacitances with the observed flow regime in the 29th column of the flattened file enabling 135000 rows as inputs to machine learning models.

5. Methods

This paper defines CXY as the normalized capacitance between electrodes X and Y, with C12, for instance, denoting the normalized capacitance between electrodes 1 and 2. The electrode counts are given in Fig.7. The classification and regression models are developed in MATLAB R2020b for this paper.

5.1 Flow Regime Identification

Flow regime identification utilizes 28 normalized capacitances from one ECT data frame as features/inputs. The associated flow regime types act as labels/outputs in machine learning (ML) classification algorithms, as illustrated in Fig. 8.

ML algorithms of Decision tree (DT), K-Nearest Neighbors (KNN), SVM and Feedforward Neural Networks (FNN) are used as flow regime classification algorithms. Classification Learner App in MATLAB is used to develop the flow regime classification algorithms of DT, KNN and SVM. The Neural Network Pattern Recognition App in MATLAB is used to develop the flow regime classification FNN algorithm.

In pursuit of enhancing model performance, another model incorporating both ECT data and differential pressure data from sensors PDT120, PDT121, and PT131 is also developed by implementing a sensor fusion method, as illustrated in Fig. 9

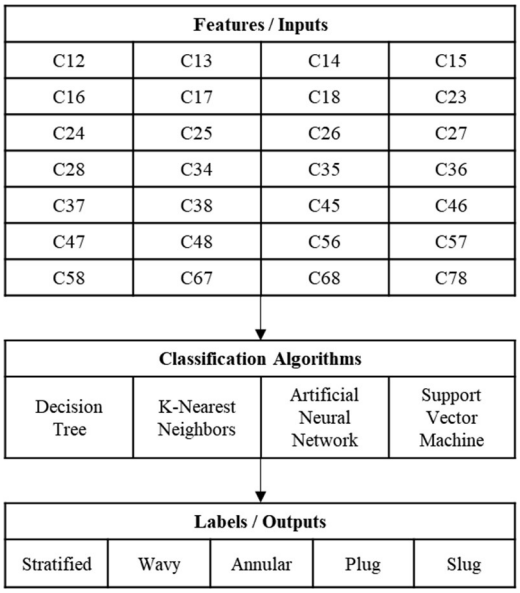

Figure 8: Model for flow regime classification using normalized capacitances as features in ML algorithms

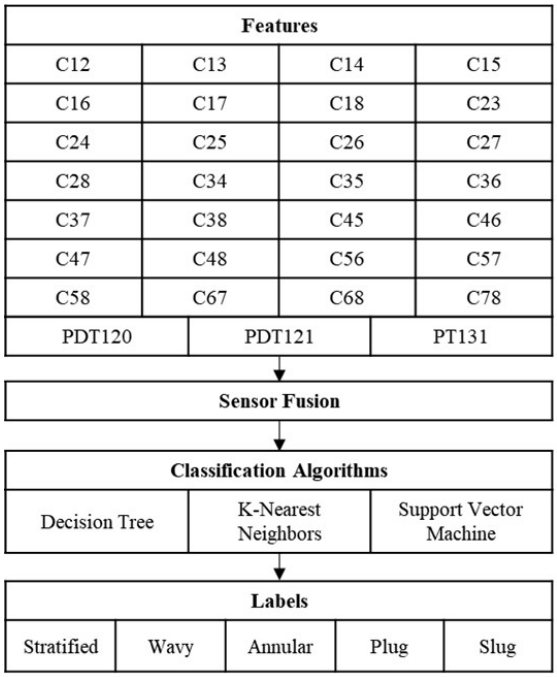

Figure 9: Model for flow regime classification using sensor fusion concept

5.2 Flow Velocity Estimation

To estimate the flow velocity, a cross-correlation analysis is performed using frames from both planes in a dual plane of ECT. The normalized capacitances at these two planes are cross-correlated to find the peak correlation lag between them. For instance, the series of C12 at plane 1 is correlated with the series of C12 at plane 2 in the ECT sensor. The peak corresponds to the degree of similarity between the two capacitances. This model specifically considers Annular, Plug, and Slug flow regimes due to their dynamic flow characteristics. The distance between the two planes mounted on the rig is 0.187 m. The flow velocity is calculated by dividing this distance by the lag time, where each lag time is 10ms.

5.3 Volume Ratio Estimation

The volume ratio for each phase is estimated by considering two differential pressure data from PDT120 and PDT121, and the inlet air flow rate data from FT131 as inputs to the regression model. The inverse volume ratio data obtained from ECT experiments is considered the model training targets, as explained in Fig. 10.

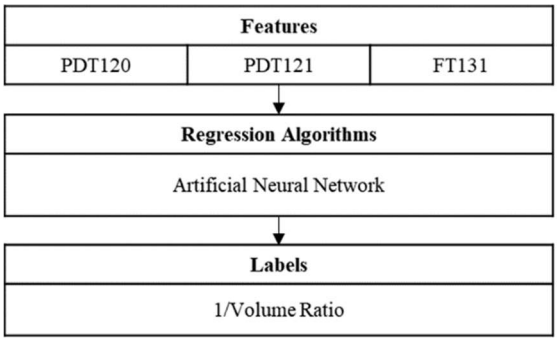

Figure 10: Model for volume ratio estimation with two pressures and flow measurement as inputs.

FNN is used as a volume ratio estimation algorithm. The trained FNN model features a single hidden layer containing 10 neurons.

6. Results

6.1 Flow Regime Identification

Using the model illustrated in Fig. 8, the flow regime classification neural network examines a total of 135000 samples with an evenly distributed array of flow regimes. For training and testing of the FNN model, these samples are divided into training, validation, and testing datasets in a 70:15:15 ratio. The hidden layer in the FNN employs a *tansig* activation function. The performance of the neural network, as seen in Fig. 11, indicates an overall accuracy of 96.5%.

KNN, SVM and DT algorithms are utilized for training flow regime classification models. Half of the data is reserved for validation purposes. Tab. 3 presents the overall validation accuracy achieved by these algorithms in classifying flow regimes.

KNN gives the highest accuracy, while SVM has the lowest accuracy among the three. The confusion matrix of KNN is shown in Fig. 12. This model will perform well when the flow is in the region of the training data as per Fig. 5. The data from transition zones of the flow regime matrix was not used to train this model.

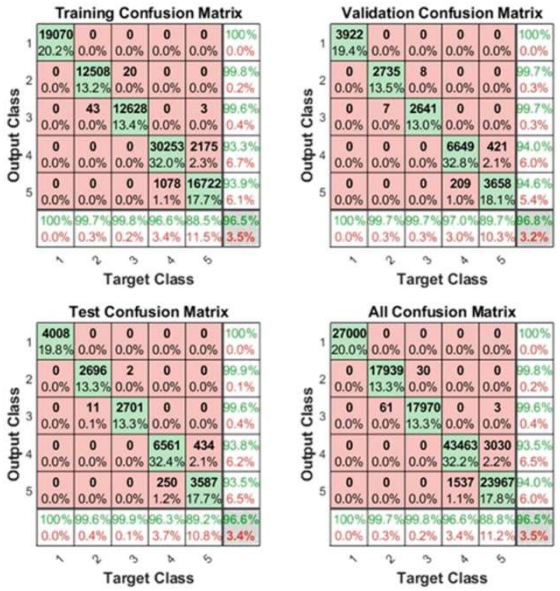

Figure 11: Performance of the FNN model for flow regime classification with 28 normalized capacitances as inputs and flow regime (1-Stratified, 2-Wavy, 3-Annular, 4-Plug, 5-Slug) as output.

Table 3: Comparison of accuracy from various flow regime identification models using 28 normalized capacitances as inputs and flow regime as output

ML algorithms	Overall accuracy (%)
KNN (Fine)	98.7
DT (Fine)	96.6
SVM (Linear)	94.7

Figure 12: Confusion Matrix of KNN (Validation) for flow regime identification with 28 normalized capacitances as inputs and flow regime as output. The corresponding sample amounts are represented by percentages and detailed in the parentheses below.

In the sensor fusion-based model, illustrated in Fig. 9, pressure and differential pressure meter signals merge with normalized capacitances to serve as features/inputs. Training of the models continues to use KNN, SVM, and DT algorithms. However, due to differing data sampling frequencies (PDT and PT sampled at 20 Hz, while ECT at 100 frames per second per plane), the total sample count is reduced for synchronization. The overall validation accuracy from these algorithms to classify flow regimes is given in Tab. 4.

Table 4: Comparison of accuracies achieved with various algorithms for flow regime identification using 28 normalized capacitances and the three pressure signals as inputs and flow regime as output

ML algorithms	Overall accuracy (%)
KNN (Fine)	98.6
DT (Fine)	98.6
SVM (Linear)	99

SVM gives the highest accuracy. The confusion matrix of SVM is shown in Fig. 13.

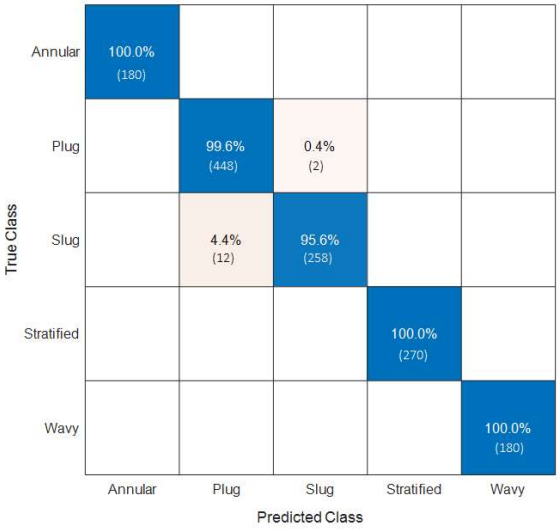

Figure 13: Confusion Matrix of SVM (Validation) for flow regime identification with 28 normalized capacitances and 3 pressure signals as inputs and flow regime as output. The corresponding sample amounts are represented by percentages and detailed in the parentheses below.

6.2. Flow Velocity Estimation

The results of estimating flow velocity are presented in the subsequent subsections, featuring two cases for each flow regime: annular, plug and slug.

6.2.1. Annular

- Case 1: Water - 2 kg/min, Air – 4 kg/min

Higher lags are disregarded as they likely arise from random fluctuations. Thus, from Tab. 5, there are 10 of found lags that are disregarded as seen marked by the orange-colored rectangles. Therefore, the domain cross-correlation lags for the remaining capacitances are at around -13, ignoring the “0” lags.

8 lags are corresponding to approximately 120 to 130ms time. Therefore, the flow velocity is estimated to be 0.187/0.13 = 1.43 m/s for this experiment.

Table 5: Cross-correlation for Water - 2 kg/min, Air – 4 kg/min (*Disregarded lags marked by the orange-colored rectangles*)

Normalized Capacitance	Peak Correlation Lag	Normalized Capacitance	Peak Correlation Lag
C12	0	C35	0
C13	0	C36	-12
C14	0	C37	-1664
C15	0	C38	-2992
C16	-13	C45	0
C17	-13	C46	-13
C18	-13	C47	-2992
C23	-175	C48	-2992
C24	0	C56	-35
C25	0	C57	-2787
C26	-12	C58	2997
C27	-2993	C67	-13
C28	-2963	C68	-13
C34	0	C78	0

- Case 2: Water - 2 kg/min, Air – 5 kg/min

Higher lags are disregarded as they likely arise from random fluctuations. Thus, from Tab. 6, there are 9 of found lags that are disregarded. Therefore, the domain cross-correlation lags for the remaining capacitances are at around -10, ignoring the "0,-1" lags. 10 lags are corresponding to approximately 60 to 100ms time. Therefore, the flow velocity is estimated to be 0.187/0.09 = 2.07 m/s for this experiment.

Table 6: Cross-correlation for Water - 2 kg/min, Air – 5 kg/min

Normalized Capacitance	Peak Correlation Lag	Normalized Capacitance	Peak Correlation Lag
C12	0	C35	0
C13	0	C36	-9
C14	0	C37	-2994
C15	-6	C38	-2997
C16	-10	C45	-1
C17	-10	C46	2997
C18	-10	C47	-2997
C23	-2997	C48	-2996
C24	0	C56	-9
C25	0	C57	-10
C26	2860	C58	-9
C27	-2994	C67	-10
C28	2997	C68	-10
C12	0	C35	0

6.2.2. Plug

- Case 1: Water - 76 kg/min, Air – 0.11 kg/min

Tab. 7 suggests the domain cross-correlation lags for the capacitances are at around -12. 28 lags are corresponding to approximately 100 to 130ms time. Hence, this experiment estimates a flow velocity of 0.187/0.12 = 1.55 m/s for this experiment.

Table 7: Cross-correlation for Water - 76 kg/min, Air – 0.11 kg/min

Normalized Capacitance	Peak Correlation Lag	Normalized Capacitance	Peak Correlation Lag
C12	-13	C35	-12
C13	-12	C36	-12
C14	-10	C37	-12
C15	-12	C38	-12
C16	-11	C45	-10
C17	-11	C46	-10
C18	-11	C47	-10
C23	-11	C48	-10
C24	-10	C56	-12
C25	-12	C57	-12
C26	-12	C58	-12
C27	-12	C67	-10
C28	-12	C68	-10
C34	-11	C78	-11

- Case 2: Water - 77 kg/min, Air – 0.07 kg/min

As seen in Tab. 8, the domain cross-correlation lags for the capacitances are at around -13, ignoring the "0, -1,-2,-3" lags. 23 lags are corresponding to approximately 100 to 150ms time. This yields a calculated flow velocity of 0.187/0.13 = 1.43 m/s.

Table 8: Cross-correlation for Water - 77 kg/min, Air – 0.07 kg/min

Normalized Capacitance	Peak Correlation Lag	Normalized Capacitance	Peak Correlation Lag
C12	-15	C35	-15
C13	-15	C36	-15
C14	-12	C37	-15
C15	-15	C38	-15
C16	-1	C45	-13
C17	-2	C46	-13
C18	-3	C47	-12
C23	-14	C48	-12
C24	-12	C56	-14
C25	-14	C57	-2
C26	-14	C58	0
C27	-14	C67	-10
C28	-14	C68	-10
C34	-13	C78	-11

6.2.3. Slug

- Case 1: Water - 75 kg/min, Air – 0.3 kg/min

Tab. 9 suggests the domain cross-correlation lags for the capacitances are at around -6. 28 lags are corresponding to approximately 50 to 70ms time. Therefore, the flow velocity is estimated to be 0.187/0.06 = 3.11 m/s for this experiment.

Table 9: Lags based on peaks of cross-correlation for Water - 75 kg/min, Air – 0.3 kg/min

Normalized Capacitance	Peak Correlation Lag	Normalized Capacitance	Peak Correlation Lag
C12	-6	C35	-6
C13	-6	C36	-6
C14	-6	C37	-6
C15	-6	C38	-6
C16	-6	C45	-6
C17	-6	C46	-6
C18	-6	C47	-6
C23	-5	C48	-6
C24	-6	C56	-7
C25	-6	C57	-7
C26	-6	C58	-7
C27	-6	C67	-5
C28	-6	C68	-5
C34	-6	C78	-6

- Case 2: Water - 77 kg/min, Air – 0.5 kg/min

Tab. 11 suggests the domain cross-correlation lags for the capacitances are at around -4. 28 lags are corresponding to approximately 30 to 50ms time. Hence, this experiment's flow velocity is estimated as 0.187/0.04 = 4.67 m/s.

The average flow velocities for three flow regimes are shown in Tab. 10. The average flow velocity of Slug regime is in the expected region. A pattern can be seen with the flow velocity increasing as the flow changes from complex flow regimes of Plug to Slug.

Table 10: Average flow velocity from cross-correlation technique on dual-plane ECT

Flow Regime	Average Flow Velocity (m/s)
Annular	1.43 to 1.87
Plug	1.24 to 1.43
Slug	2.67 to 3.74

6.3 Volume Ratio Estimation

In the volume ratio estimation FNN model, a total of 1350 samples are used for training and testing. These samples are partitioned into training, validation, and testing datasets with a 70:15:15 ratio. The activation function in the hidden layer is *tansig,* and in the output layer is linear. The model's performance, shown in Fig. 14, achieves an R-value of 0.95 for the test dataset, with an overall R-value also standing at 0.95. Some of the outputs are far from the target since the regression model is not perfect and has an R^2 value of 0.9. This model can be used to estimate the volume ratio in the pipe with good confidence.

Table 11: Cross-correlation for Water - 77 kg/min, Air – 0.5 kg/min

Normalized Capacitance	Peak Correlation Lag	Normalized Capacitance	Peak Correlation Lag
C12	-5	C35	-4
C13	-4	C36	-4
C14	-4	C37	-4
C15	-4	C38	-4
C16	-4	C45	-4
C17	-4	C46	-5
C18	-4	C47	-4
C23	-3	C48	-4
C24	-4	C56	-4
C25	-4	C57	-4
C26	-5	C58	-4
C27	-5	C67	-4
C28	-5	C68	-4
C34	-5	C78	-4

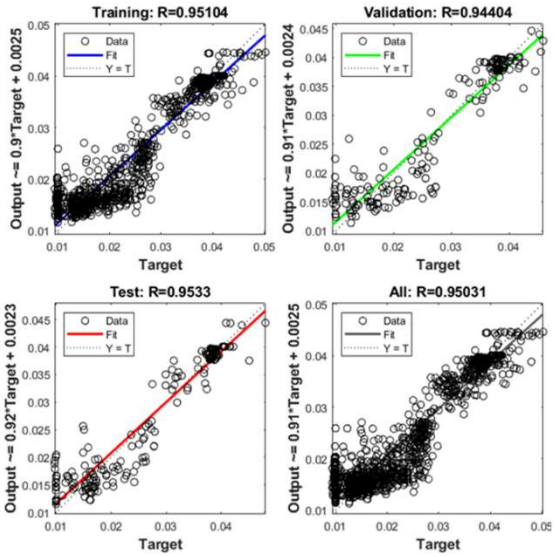

Figure 14: Performance of volume ratio estimation model with PDT120, PDT121 and FT131 as inputs and 1/Volume Ratio from ECT as output

7. Summary and Discussions

The data-driven multiphase flow metering models developed, capable of classifying flow regimes and estimating phase fractions and velocities for two-phase air/water flow, are developed after collecting ECT data from the horizontal flow rig located at USN.

The flow regime classification model, using ECT, achieved an accuracy surpassing 94%. Additionally, a sensor fusion model integrating ECT and pressure sensor data for flow regime classification exceeded 98% accuracy. For annular, plug and slug regimes, flow velocity was estimated using cross-correlation. The volume ratio estimation neural network model attained an R-value greater than 0.95.

This paper demonstrates the feasibility of multiphase flow metering through the use of ECT and pressure sensor data. As depicted in Fig. 15, the data acquired from these sensors can be directly channelled into dedicated ML algorithms to provide insights into multiphase flow in pipeline. This approach facilitates the monitoring and control of processes involving multiphase flow with real time processing of process data on premises or in the enterprise cloud.

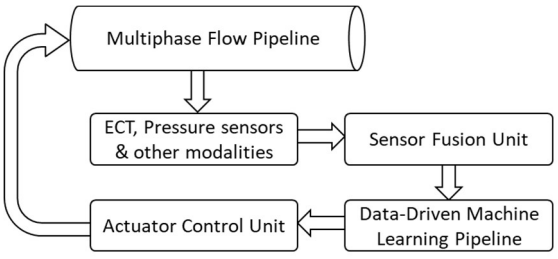

Figure 15: An algorithm for actuator control using a data-driven ML metering model.

Applying ML algorithms to time-series data from these sensors eliminates the necessity for complex mathematical time-series and image-processing methods.

Acknowledgment
Many thanks to Fredrik Hansen of USN for his support in the operation of the multiphase flow rig. This work is closely coupled to an ongoing project SAM (SAM: Self Adapting Model-based system for Process Autonomy - SINTEF), with Equinor and SINTEF as the major partners.

References

Almalki, N., Ahmed, W.H., 2020. Prediction of two-phase flow patterns using machine learning algorithms. https://doi.org/10.11159/ffhmt20.182

Alssayh, M., Addali, A., David, Dao, T., 2013. Identification Of Two Phase Flow Regime Using Acoustic Emission Technology.

Dupré, A., Ricciardi, G., Bourennane, S., Mylvaganam, S., 2017. Electrical Capacitance-Based Flow Regimes Identification—Multiphase Experiments and Sensor Modeling. IEEE Sens. J. 17, 8117–8128. https://doi.org/10.1109/JSEN.2017.2707659

Godfrey Nnabuife, S., Kuang, B., Whidborne, J.F., Rana, Z., 2021. Non-intrusive classification of gas-liquid flow regimes in an S-shaped pipeline riser using a Doppler ultrasonic sensor and deep neural networks. Chem. Eng. J. 403, 126401. https://doi.org/10.1016/j.cej.2020.126401

H. L. M. Ameran, E. J. Mohamad, R. A. Rahim, W. N. A. Rashid, M. M. Mohamad, H. Hashim, Z. Zakaria, M. F. Shaib, O. M. F. Marwah, 2015. Velocity Measurement Simulative Study Of Twin Plane ECT Using Advanced Cross Correlation Technique. ARPN J. Eng. Appl. Sci., 19 10. https://doi.org/October 2015

Hansen, L.S., Pedersen, S., Durdevic, P., 2019. Multi-Phase Flow Metering in Offshore Oil and Gas Transportation Pipelines: Trends and Perspectives. Sensors 19, 2184. https://doi.org/10.3390/s19092184

Jayanti, S., 2011. Wavy Flow. Begel House Inc. https://doi.org/10.1615/AtoZ.w.wavy_flow

Liné, A., Fabre, J., 2011. Stratified Gas-Liquid Flow. Begel House Inc. https://doi.org/10.1615/AtoZ.s.stratified_gas-liquid_flow

Noorain Syed Kazmi, 2023. Multiphase Flow Metering with Multimodal Sensor Suite for Identification of Flow Regimes, and Estimation of Phase Fractions and Velocities. University of South-Eastern Norway, Porsgrunn, Norway.

Pereyra, E., Torres, C., Mohan, R., Gomez, L., Kouba, G., Shoham, O., 2012. A methodology and database to quantify the confidence level of methods for gas–liquid two-phase flow pattern prediction. Chem. Eng. Res. Des. 90, 507–513. https://doi.org/10.1016/j.cherd.2011.08.009

Process Tomography Limited, 2011. Electrical Capacitance Tomography System Type TFLR5000 Operating Manual.

Saied, I., Meribout, M., 2016. Electronic hardware design of electrical capacitance tomography systems. Philos. Trans. R. Soc. Math. Phys. Eng. Sci. 374, 20150331. https://doi.org/10.1098/rsta.2015.0331

Soo, S.L., 1990. Multiphase fluid dynamics. Science Press ; Gower Technical, Beijing : Aldershot ; Brookfield, USA.

Stavland, S.H., Arellano, Y., Hunt, A., Maad, R., Hjertaker, B.T., 2021. Multimodal Two-Phase Flow Measurement Using Dual Plane ECT and GRT. IEEE Trans. Instrum. Meas. 70, 1–12. https://doi.org/10.1109/TIM.2020.3034615

Tan, C., Dong, F., 2023. Sensor Instrumentation for Flow Measurement, in: Narayan, R. (Ed.), Encyclopedia of Sensors and Biosensors (First Edition). Elsevier, Oxford, pp. 536–554. https://doi.org/10.1016/B978-0-12-822548-6.00074-1

Vohr, J.H., 1960. Flow Patterns Of Two-Phase Flow–A Survey Of Literature (No. TID-11514; CU-2-60-AEC-187-Ch.). Columbia Univ., New York. Engineering Research Labs.

Wang, H.X., Zhang, L.F., 2009. Identification of two-phase flow regimes based on support vector machine and electrical capacitance tomography. Meas. Sci. Technol. 20, 114007. https://doi.org/10.1088/0957-0233/20/11/114007

Zeigarnik, Y.A., 2011. Annular flow. Begel House Inc. https://doi.org/10.1615/AtoZ.a.annular_flow